Appendix 1

SPECIMEN CATALOGUE

Specimens referred to by six-digit numbers are held by the Geology Department, University of Tasmania. Specimens referred to by five-digit numbers with a hyphen between the second and third digits (e.g. 77-382) are held by the Department of Mines, Tasmania. Code for specimen preparation:

H	hand specimen	Pt	polished thin section
T	thin section	C	crushed rock
P	polished section	Py	pyrite concentrate

Specimen Number	Rock type	Location[1]	Preparation
75-380A	Chloritic lithic tuff, massive pyroclastics.	DDH71R, 128½'	HT
75-380B	"	DDH71R, 128½'	HT
75-381	Quartz-phyric snowflake-texture rhyolite intrusive(?).	DDH71R, 362'	HT
75-382	Crystal lithic tuff with shale fragments, massive pyroclastics.	DDH71R, 773'	HT
75-384	Vitric tuff with quartz ovoids, massive pyroclastics.	DDH71R, 1199'	HT
75-384A	Crystal-lithic tuff, massive pyroclastics.	DDH71R, 1199'	HT
75-385	Interbedded crystal tuff and mudstone, massive pyroclastics.	DDH71R, 1717'	HT
75-386	Vitric-crystal ruff, host rock.	DDH71R, 1735'	HT
75-387	Vitric-crystal tuff, host rock.	DDH71R, 1776'	HT
75-388	Quartz-feldspar porphyry intrusive.	DDH71R, 2042½'	HT
75-594	Tuffaceous sandstone, Chamberlain Shale.	7756E 7472N	HT
75-599	Siltstone, Chamberlain Shale.	7779E 7457N	HT
75-602	Crystal tuff, Chamberlain Shale.	7788E 7448N	HT
75-605	Snowflake rhyolite, massive pyroclastics.	7858E 7634N	HT
75-606	Snowflake-texture rhyolite intrusive(?).	DDH71R, 530'	HT
75-607	"	DDH71R, 278'	HT
75-650B	Ash-flow tuff, footwall pyroclastics.	7766E 7139N	HT
75-652	Crystal-vitric tuff, massive pyroclastics.	7792E 7268N	HT
75-653	Massive quartz-sericite rock	7796E 7310N	HT
75-656	Vitric ash-flow tuff.	7814E 7190N	HT
75-661	Vitric-crystal ash-flow tuff, footwall pyroclastics.	7659E 6760N	HT

Specimen Number	Rock Type	Location[1]	Preparation
75-747	Micaceous sandstone.	7515E 6764N	HT
75-748	Crystal-lithic tuff, massive pyroclastics.	7530E 6767N	HT
75-749	Crystal-lithic tuff, massive pyroclastics.	7541E 6776N	HT
75-750	Porphyry fragment in 75-749.	7541E 6776N	T
75-746	Volcaniclastic sandstone, Chamberlain Shale correlate(?) west of Hercules.	7514E 6763N	HT
75-754	Crystal-vitric tuff, footwall pyroclastics.	7891E 7146N	HT
75-755	Sericite schist, footwall pyroclastics.	7885E 7194N	HT
75-763	Vitric tuff with quartz ovoids, massive pyroclastics.	DDH71R, 1183½'	HT
75-764	Carbonate-rich slate, black slate.	DDH71R, 1508'	HT
75-765	Welded vitric-crystal tuff, footwall pyroclastics.	DDH71R, 2227'	HT
75-766	Quartz-feldspar porphyry intrusive.	DDH71R, 1932'	HT
75-767	Sericitic siltstone, host rock.	DDH71R, 2124'	HT
75-769	Lithic-crystal tuff, massive pyroclastics.	DDH71R, 1280'	HT
75-771	Welded vitric-crystal tuff, massive pyroclastics.	DDH71R, 2356'	HT
75-773	Unwelded vitric-crystal tuff, massive pyroclastics, Hercules area.	DDH H950, 1094'	HT
76-281	Black slate, Stitt Quartzite.	7741E 7846N	HT
76-282	Sandstone, Stitt Quartzite.	77372E 78455N	HT
76-283	Conglomerate, Stitt Quartzite.	7734E 78405N	HT
76-284	Laminated sandstone, Stitt Quartzite.	77265E 7840N	HT
76-285	Cross-bedded sandstone, Stitt Quartzite.	77265E 7840N	HT
76-286	Siltstone, Stitt Quartzite.	77515E 7837N	HT
76-290	Siltstone, Westcott Argillite.	7669E 77605N	HT
76-290A	"	7669E 77605N	HT
76-291	Sandstone, Stitt Quartzite.	7713E 78195N	HT
76-292	"	77185E 7824N	HT
76-293	"	77185E 7824N	HT
76-294	"	77185E 7824N	HT
76-295	"	77185E 7824N	HT
76-296	"	77185E 7824N	HT
76-297	Sandstone, base of bed.	77185E 7824N	HT
76-298	Sandstone, top of bed.	77185E 7824N	HT
76-300	Sandstone/shale, Westcott Argillite.	7695E 7806N	HT
76-301	Slide conglomerate, Westcott Argillite.	7695E 7806N	HT
76-302	"	7684E 7786N	HT
76-306	Sandstone, Westcott Argillite corr.	76335E 77415N	HT
76-307	Dolomicrite, Westcott Argillite.	76300E 77388N	HT
76-316	Brecciated slate, Stitt Quartzite.	7751E 78455N	HT
76-322	Sandstone, Westcott Argillite correlate.	7632E 7743N	HT
76-324	Dolerite clast in conglomerate, Westcott Argillite correlate.	7629E 7741N	HPtT
76-325	Quartzwacke, Munro Creek Fm.	7610E 7732N	HT
76-326	Laminated fine-grained sandstone, Crimson Creek Fm.	75903E 77079N	HT

Specimen Number	Rock Type	Location[1]	Preparation
76-327	Sandstone, Crimson Creek Fm.	7586E 77015N	HT
76-328	"	7585E 7697N	HT
76-333	Volcaniclastic siltstone, Crimson Creek Fm.	75835E 7676N	HT
76-334	Sandstone, Crimson Creek Fm.	7581E 76256N	HT
76-338	Quartzwacke, Munro Creek Fm.	76065E 76035N	HT
76-339	"	76097E 76022N	HT
76-342	Sandstone, Munro Creek Fm.	76177E 7732N	HT
76-348	Grey siltstone/black slate, Munro Creek Fm.	76445E 7576N	HT
76-349	Dolomite, Westcott Argillite corr.	7672E 75176N	HT
76-352	Interbedded sandstone/black shale, Stitt Quartzite correlate.	7699E 75205N	HT
76-353	Laminated sandstone/shale, Stitt Quartzite correlate.	7699E 75205N	HT
76-354	Cross-laminated, convoluted sandstone, Stitt Quartzite correlate.	7699E 75205N	HT
76-355	Cross-laminated sandstone, shale Stitt Quartzite correlate.	7699E 75205N	HT
76-368	Sericitic vitric crystal tuff with K-feldspar, footwall pyroclastics.	78602E 73042N	HT
76-371	Quartz-phyric altered tuff, massive pyroclastics.	78172E 72565N	HT
77-2	Vitric-crystal tuff, footwall pyroclastics.	7743E 6835N	HTC
77-3	"	7783E 7023N	HTC
77-699	Base of sandstone bed in black slate.	7859E 7498N	HT
77-700	Top of sandstone bed in black slate.	7859E 7498N	HT
77-701	Lithic tuff, massive pyroclastics.	78584E 75076N	HT
77-132	Graded sandstone bed.	DDH MDR1, 19.02m	HT
77-133	Graded sandstone.	" 19.02m	HT
77-134	Siltstone.	" 27.11m	HT
77-135	Sandstone-mudstone.	" 38.0m	HT
77-136	Siltstone-mudstone.	" 38.3m	HT
77-137	Graded sandstone.	" 39.9m	HT
77-138	Dolomitic siltstone.	" 51.80m	HT
77-139	Cleaved sandstone-mudstone.	" 56.86m	HT
77-140	Conglomerate with chert clasts.	" 64.09m	HT
77-141	Graded siltstone-shale.	" 78.06m	HT
77-142	Graded conglomerate-sandstone.	" 71.86m	HT
77-143	Graded conglomerate-sandstone.	" 71.86m	HT
77-144	Vitric-lithic tuff with pyritic black shale fragment.	" 211.95m	HT
77-145	Chlorite-flecked vitric-crystal tuff.	" 218.10m	HT
77-146	Quartz-feldspar crystal-lithic tuff.	" 223.70m	HT
77-147	Cleaved tuff.	" 226.5m	HT
77-148	Schistose vitric-lithic tuff.	" 229.3m	HT
77-149	Fine-grained vitric-lithic tuff.	" 242.57m	HT
77-150	Cleaved vitric-lithic tuff.	" 249.24m	HT
77-151	Vitric-lithic tuff.	" 266.83m	HT
77-152	Carbonate-veined vitric crystal tuff.	" 277.59m	HT
77-153	Chloritized lithic tuff.	" 281.3m	HT

Specimen Number	Rock type	Location[1]	Preparation
77-154	Vitric-lithic-crystal tuff with chloritic fragments.	DDH MDR1, 282.76m	HT
77-155	Vitric-crystal tuff with shale fragments.	" 289.95m	HT
77-156	Conglomerate.	98m	HT
77-157	Base of sandstone bed.	" 98.3m	HT
77-158	Top of sandstone bed.	" 98.5m	HT
77-159	Crystal-vitric tuff (base of bed).	" 101m	HT
77-160	Crystal-citric tuff (top of bed).	" 101.91m	HT
77-162	Lithic tuff.	" 103.24m	HT
77-163	"	" 104.9m	HT
77-164	Conglomerate.	" 113.58m	HT
77-165	"	" 154.4m	HT
77-166	Conglomerate clast in tuff, contact zone.	" 184.2m	HT
77-167	Chlorite-flecked schist.	" 187.4m	HT
77-168	Tuff.	" 191.5m	HT
77-169	"	" 192.6m	HT
83-1	Salisbury Conglomerate.	76385E 7743N	HT
83-2	Vitric-crystal tuff, massive pyroclastics, Hercules.	DDH H955, 310'	HT
83-3	Siltstone, Westcott Argillite.	7680E 7777N	HT
83-4	Conglomerate, Westcott Argillite.	7696E 7800N	HT
83-5	"	7677E 7772N	HT
83-6	Vitric crystal tuff, massive pyroclastics.	7929E 7556N	HT
83-7	"	7908E 7240N	C
83-8	Andesitic tuff, massive pyroclastics.	7770E 6689N	C
83-9	Rhyolite lava, Mt Black Volcanics.	8000E 8019N	C
83-10	Vitric-crystal tuff, footwall pyroclastics.	7657E 6757N	C
105111	Quartz sericite schist trace pyrite, Rosebery mine.	DDH R950, 241	HPy
112	Quartz-sericite-pyrite schist.	DDH R1002, 441	Py
113	Quartz-sericite-chlorite schist, trace pyrite.	DDH R1016, 241	Py
114	Quartz-sericite schist, trace pyrite and chalcopyrite.	DDH R1155, 81	Py
115	Quartz-sericite-pyrite schist.	DDH R1163, 486	PyPt
116	Quartz-sericite schist, trace pyrite.	DDH R1174, 610	HPy
117	"	DDH R1176, 96	Py
118	Quartz-sericite schist, trace pyrite.	DDH R1206, 75	HPy
119	Quartz-sericite-carbonate-pyrite schist.	DDH R1254, 109	PyPt
120	Quartz-sericite-chlorite-pyrite schist.	DDH R1254, 175	Py
121	Quartz-sericite-pyrite schist.	DDH R1255,248	PtPy
122	Quartz-sericite schist, trace pyrite.	DDH R1256, 91	HPy
123	Quartz-sericite-pyrite schist.	DDH R1272, 168	HPy
124	Quartz-sericite-chlorite-pyrite schist.	DDH R1281,1139	Py
125	Quartz-sericite schist, trace pyrite.	DDH R1285, 393	HPY

Specimen Number	Rock type	Location[1]	Preparation
105126	Quartz-chlorite-sericite schist, trace pyrite.	DDH R1304, 1162	Py
127	Quartz-sericite schist, trace pyrite, chalcopyrite.	DDH R1336, 28	Py
128	Quartz-sericite schist, trace pyrite, sphalerite.	DDH R1340, 336	Py
129	Quartz-sericite-pyrite schist, albite-chalcopyrite vein.	DDH R1351, 923	HPyPt
130	Quartz-sericite schist, trace pyrite.	DDH R1360, 935	Py
131	Quartz-sericite-chlorite schist, trace pyrite, chalcopyrite.	DDH R1388, 1037	Py
132	Quartz-chlorite schist with tourmaline, trace pyrite.	DDH R1399, 759	HPtPy
133	Quartz-chlorite-sericite-pyrite schist.	DDH R1406, 800	Py
134	Quartz-sericite schist, trace pyrite.	DDH R1406, 915	PyPt
135	Quartz-sericite-pyrite schist.	DDH R1418, 824	HPy
136	Quartz-sericite schist, trace pyrite.	DDH R1452, 922	HPy
137	Quartz-sericite-pyrite schist with pyrite-chalcopyrite veins.	DDH R1452, 958	HPyPt
138	Quartz-chlorite-pyrite schist.	DDH R1485, 1045	HPy
139	Quartz-sericite-chlorite schist, trace pyrite.	DDH R1500, 1011	HPy
140	Quartz-sericite-pyrite schist.	DDH R1609, 852.	PtPy
141	Quartz-sericite schist, trace pyrite.	DDH R1650, 880	Py
142	Quartz-sericite-pyrite schist with galena, sphalerite, tourmaline.	DDH R1650, 943	Pt(2)Py
143	Quartz-sericite schist, trace pyrite.	DDH R1651, 1064	HPy
144	Quartz-sericite-chlorite schist, trace pyrite.	DDH R1651, 1073	HPy
145	Quartz-sericite-chlorite-pyrite schist, carbonate veins.	DDH R1661, 883	HPtPy
146	Quartz-sericite schist, trace pyrite.	DDH R1700, 990	HPy
147	Quartz-sericite-chlorite-pyrite schist.	DDH R1716, 905	HPtPy
148	Quartz-sericite-pyrite schist.	DDH R1770, 1819	PyPt
149	Pyritic sericite-chlorite-quartz schist with sphalerite and galena.	DDH R1830, 1709	HPyPt
150	Chlorite-quartz-sericite-garnet-biotite-tourmaline-pyrite-sphalerite schist.	DDH R1840, 1767	HPyPt
151	Quartz-sericite-pyrite schist with chalcopyrite.	DDH R1920, 1939	PyPt
152	Quartz-sericite-pyrite-chalcopyrite schist.	DDH R1971, 210	Py
153	Quartz-sericite-carbonate-pyrite schist.	DDH R1982, 245	PyPt
154	Quartz-sericite-pyrite schist.	DDH R2037, 443	HPy
157	Pyritic quartz-sericite schist.	20N 2630E RL8125	C
158	Pyritic sericite-chlorite-quartz schist.	475N 1120E, RL9076	C

Specimen Number	Rock type	Location[1]	Preparation
105159	Sericite-quartz schist, trace pyrite.	283N 1195E, RL9405	C
160	Pyritic quartz-chlorite-sericite schist.	100S 1780E, RL620	C
161	Banded pyritic ore.	700N 1008E,RL9664	HPt
162	"	700N 1002E,RL9664	HP
163	Sericite schist with arsenopyrite.	700N 996E,RL9664	HPt
164	Banded pyritic ore.	700N 990E,RL9664	HPt
165	"	700N 984E,RL9664	HPt
166	"	700N 972E,RL9664	HPt
167	"	700N 966E,RL9664	HPt
168	Banded sphalerite-rich ore.	700N 960E,RL9664	HPt
169	Compact pyrite-chalcopyrite.	700N 954E,RL9664	HP
170	"	700N 942E,RL9664	HP
171	"	700N 936E,RL9664	HPt
172	Banded pyrite-chalcopyrite.	700N 930E,RL9664	HPt
173	Chlorite schist.	700N 912E,RL9664	HPt
174	Banded sphalerite-rich ore.	760N RL9512	HPt
175	Banded pyritic ore.	700N RL9512	HP
176	"	700N RL9512	HPt
177	"	700N RL9512	HPt
178	Compact sphalerite-galena ore.	700S 1030E,RL9700	HP
179	"	700S 1021E,RL9700	HP
180	"	700S 1018E,RL9700	HPt
181	"	700S 1015E,RL9700	HPt
182	Banded baritic ore.	627N 1799E,RL9235 DDH R1500, 669	HPt
183	"	626N 1796E,RL9251 DDH R1500, 673	HPt
105190	Crystal lithic tuff, massive pyroclastics.	7876E 7516N	HT
76-745	Massive pyrite-pyrrhotite.	DDH R2785[2], 133	HP
76-746	Massive pyrrhotite - sphalerite.	DDH R2785, 135¼	HP
76-747	Massive pyrrhotite-pyrite.	DDH R2785, 133¾	HP
76-748	Massive coarse-grained sphalerite-galena-pyrite.	DDH R2791, 160½	HP
76-750	Massive pyrrhotite-pyrite.	DDH R2791[3], 161½	HP
76-751	Banded pyrite-chalcopyrite-sphalerite ore.	G lens, 15 level	HP
76-752	Pyrite-magnetite-chalcopyrite-hematite.	130N 1250E,RL9664	H(2)P

1 Locations of specimens 76-745 to 76-752, 105111-105188 are in terms of the Rosebery mine grid, distances in feet.
Remainder of specimens located in terms of Australian metric grid, 100 000 metre square CP, following the convention of the Department of Lands, Tasmania 1:100 000 sheet 8014 Sophia (1977). Most specimens are located to a nominal 10 metres.

2 Collar location 405S 1347E, RL9364, bearing 92½°, -5° dip.

3 Collar location 425S 1344E, RL9365, bearing 137°, -1° dip.

Appendix 2

ROSEBERY DRILL HOLE

In 1976, a drill hole, proposed by the writer, was drilled beneath the Natone Volcanics by the Department of Mines. The primary purpose of the drill hole was to obtain fresh samples of the Natone Volcanics for age dating. Unfortunately strong alteration and cleavage development and the presence of black shale clasts throughout rendered the unit unsuitable for Rb-Sr and U-Pb dating respectively. The secondary purpose was to clarify facing relationships in this part of the Rosebery Group which is poorly exposed in the Natone Creek area compared with the Pieman Gorge section to the north. This object was successfully achieved and demonstrated that, as to the north, part of the Rosebery Group section faced east and was largely responsible for the revision of the stratigraphy of the Rosebery Group suggested in this thesis.

Collar location:	Eastern side of Natone Creek; 76415E 71062N.
Direction and dip of hole:	083^{o}, -45^{o}
Depth:	290.16 m.

Depth (m)	DRILL LOG
0-3.87	No core recovery. Hole collared at contact between deeply weathered quartz-phyric pyroclastics and slate.
3.87-7.27	Broken core; massive pink clay with sparsely disseminated 1 mm quartz grains. Possible tuff.
7.27-61.87	Interbedded grey-green dolomitic coarse- to fine-grained sandstone and laminated cream mudstone. Intercalated conglomerate beds at 7.87-9.5 m, 15.43-15.93 m, 27-31.22 m and 39.2-39.5 m consist of clasts of white to reddish chert, maroon mudstone and lithic wacke, fuchsite, mafic volcanic and dolerite clasts on average 1-2 cm in diameter in a sandy matrix. The framework is open. Bedding/core axis

Depth (m)	DRILL LOG
	angle = 45°, cleavage is subparallel to bedding. A breccia with angular fragments is present at 59.52-59.62 m. Folds are present at 27.45 m, 31.45-43 m, particularly at 37-39 m. Graded bedding indicates downhole (east) facings at 54.19, 57.0, 59.9 and 60.6 m. Pyrite and chalcopyrite are disseminated in carbonate veins (1 cm thick) at 61.45 and 61.75 m.
61.87-73.2	Conglomerate. Similar to that between 27.0 and 31.22 m except that clasts are more widely spaced and a higher proportion of grey to white chert clasts is present. Suggestion of vague downhole grading at 61.87-67.52 m, but this is an overall impression as the conglomerate consists of a number of amalgamated beds with rapid changes in grainsize.
73.2-84.58	Sandstone-mudstone sequence similar to that between 31.22 and 61.87 m. Graded bedding indicates downhole (east) facings at 76.50, 76.59, 77.93 and 78.1 m.
84.58-101.01	Conglomerate, with lower proportion of chert clasts than between 61.87 and 73.2 m, containing intercalated sandstone and grit lenses from less than 10 cm to 20 cm thick. Graded bedding in grit to sandstone lens at 98.3 m indicates downhole facing. Between 90 and 100 m chert clasts comprise 25% of the rock, carbonate clasts are also abundant and fuchsite clasts are rare. Contacts between sandy and pebbly units are subparallel to cleavage. Some disseminated fine-grained pyrite at 97 m.
101.01-104.87	Felsic tuff consisting of a number of sub-units. 101.01-101.93: fine-grained, cleaved, vitric crystal tuff with decrease in proportion of crystals downhole. 101.93-102.04: medium-grained quartz-feldspar bearing vitric crystal tuff. Contains one 0.5 cm pyrite fragment. Contact with next unit slightly discordant (10°) to cleavage. Carbonate veining along contact. 102.04-104.87: Two units of lithic-vitric crystal tuff, coarse- to medium-grained with pronounced fabric parallel to cleavage. Sub-unit from 103.14-104.87 m shows downhole grading involving decrease in size and abundance of subequant lithic clasts.

Depth (m)	DRILL LOG
104.87-182.5	Polymict matrix-supported conglomerate containing clasts, up to 5 cm in diameter, of quartzose sandstone, chert, black shale, carbonate and fuchsite in a sandstone matrix. A number of grit to medium-grained and rarely mudstone intercalations are present. Graded bedding in some of these indicates downhole facing. Broken core between 123.6-123.9 m, 127.7-127.9 m, 147.9-148.4 m, 165.3-166.4 m, 170-171.45 m, 174.5-178.8 m. In a number of these zones are vuggy quartz carbonate veins with minor pyrite. At 107 m, bedding/core axis angle is 65^{o}.
182.5-290.16	Felsic tuff. At 184.2 m a conglomerate fragment 5 cm in diameter with irregular margins occurs in the tuff, confirming the numerous indications of downhole facing noted above. The conglomerate clast is identical to the conglomerate uphole At 198 m the dominant cleavage is at 80^{o} to the core axis, a weaker cleavage at 60^{o} is present. To 187.3 m strongly cleaved sericitic vitric-lithic tuff with scattered 1-2 mm quartz and feldspar phenocrysts is present. The feldspars are sericitized. Lithic fragments up to 3 cm long consist of both equant and flattened volcanic rocks, and sedimentary rocks, predominantly black slate clasts ranging upward in size from 1 mm. This is the dominant rock type present in the tuff. 187.3-188.3 m: Cleaved unit with 2-4 mm ellipsoidal chlorite blebs in a pale green sericitic matrix. Minor carbonate and trace pyrite are present. 188.3-211.95 m: Similar rock type to 182.5-187.3 m. Brecciated zone with chlorite veinlets from 198.0-198.5 m. Around 211 m is a zone rich in black slate fragments. 211.95-219.58 m: Chloritic unit similar to that between 187.3-188.3 m. Disseminated zones of fine pyrite euhedra 0.5-1.0 cm in diameter are present. 219.58-220.45 m: Quartz-sericite schist with 3 mm rounded siliceous blebs. (In thin section these display a granophyric texture.) 220.45-222.65 m: Chloritic unit as above. 222.65-229 m: Unit of vitric-crystal-lithic tuff with quartz and feldspar phenocrysts more abundant and coarser (3-4 mm)

Depth (m)	DRILL LOG
	than those above. Black slate, quartzite and chert fragments up to 3 cm thick are abundant throughout. Irregular, occasionally folded carbonate veins present. Schistosity/core axis angle 80°.
	229-230 m: Quartz-sericite schist with spaced cleavage.
	230-237 m: Fine tuff with few phenocrysts and finer black slate fragments 0.5 cm in diameter.
	237-250.5 m: Coarse-grained vitric-crystal-lithic tuff similar to that between 222.65 and 229 m.
	250.5-278.12 m: Pale grey aphyric finer-grained tuff. Black slate clasts to 3 cm in length (e.g. at 263.80 m). Numerous brown-weathering sideritic carbonate veins.
	278.12-290.16 m: Vitric-crystal-lithic tuff similar to that between 222.65 and 229 m. Chloritized zone at 280.96-283.2 m.
290.16	End of hole.

Appendix 3

PYRITE SEPARATION

The following procedure, developed by P. O'Dwyer, a metallurgist of the E.Z. Company, was used in separating pyrite from core samples of the footwall schist.

Grinding

Up to 1 kg of coarsely crushed core and 330 ml of water was ground for 15 to 20 minutes in a laboratory-size rod mill. The pulp was wet-screened through a 100# sieve and the finer fraction used for pyrite concentration.

Flotation

Flotation was carried out in a 1.25 l Denver cell.

(i) Copper conditioning was carried out for 5 minutes with 10 ml of 0.5% NaCN and sufficient lime to raise the pH to 11.5 was added. 30 sec before the end of this stage, 3 drops of cresylic acid and 5 ml of 0.5% of sodium aerofloat were added.

(ii) A rougher copper float was carried out for 2 minutes to remove chalcopyrite.

(iii) Pyrite scrubbing was carried out for 11 minutes after the cell was topped-up with water to the 1.25 l mark, and sufficient H_2SO_4 was added to maintain the pH at 4.5 during this stage.

(iv) Pyrite conditioning was carried out for 11 minutes following addition of 6.7 ml of 1% sodium isopropyl xanthate.

(v) A pyrite rougher float was carried out for 75 secs after addition of 2 drops of M.I.B.C. to promote frothing.

(vi) A pyrite cleaner float using the material from the pyrite rougher float was carried out after addition of 2 drops of M.I.B.C. for 1 minute or until the colour of the froth indicated impurities in the pyrite recovered.

(vii) A pyrite recleaner float was carried out using the concentrate from the pyrite cleaner flotation. 3.5 ml of 1% sodium isopropyl xanthate and 2 drops of M.I.B.C. were added and flotation was stopped after 30 secs. A final concentrate greater than 99.5% pure was achieved by the above process.

APPENDIX 4

THERMODYNAMIC DATA

The standard state chosen for solids and liquids is the pure substance at the pressure and temperature of interest. The standard state for gases is the ideal gas at temperature and a pressure of 1 bar.

(a) DATA USED IN CONSTRUCTING FIGS 7.2-7.4

		T°C	Psat	1 kbar	2 kbar
1.	$Mg_5Al_2Si_3O_{10}(OH)_8 + \frac{5}{7}Fe_5^{2+}Fe_2^{3+}Si_3O_{10}(OH)_8 + \frac{25}{21}SiO_2 + \frac{10}{21}H_2O_{(l)} = Fe_5^{2+}Al_2Si_3O_{10}(OH)_8 + \frac{5}{6}Mg_6Si_4O_{10}(OH)_8 + \frac{5}{4}O_{2(g)}$	250	-16.094	-16.067	-16.045
		300	-14.593	-14.561	-14.538
		350	-13.343	-13.308	-13.279
2.	$Fe_5^{2+}Al_2Si_3O_{10}(OH)_8 + \frac{1}{4}O_{2(g)} = Fe_4^{2+}Fe^{3+}Al_2Si_3O_{11}(OH)_7 + \frac{1}{2}H_2O_{(l)}$	250	11.139	11.027	10.917
		300	10.006	9.901	9.796
		350	9.062	8.964	8.861
3.	$Mg_5Al_2Si_3O_{10}(OH)_8 + \frac{5}{7}Fe_5^{2+}Fe_2^{3+}Si_3O_{10}(OH)_8 + \frac{3}{7}Fe_5^{2+}Al_2Si_3O_{10}(OH)_8 + \frac{25}{21}SiO_2 = \frac{10}{7}Fe_4^{2+}Fe^{3+}Al_2Si_3O_{11}(OH)_7 + \frac{5}{6}Mg_6Si_4O_{10}(OH)_8 + \frac{5}{21}H_2O_{(l)}$	250	-0.181	-0.314	-0.449
		300	-0.299	-0.417	-0.543
		350	-0.398	-0.502	-0.621
4.	$Fe_5^{2+}Fe_2^{3+}Si_3O_{10}(OH)_8 + 7FeS_2 = 14FeS + 3SiO_2 + 4H_2O_{(l)} + 4O_{2(g)}$	250	-157.20	-157.46	-157.67
		300	-137.45	-137.73	-137.96
		350	-120.73	-121.04	-121.40
5.	$Fe_5^{2+}Fe_2^{3+}Si_3O_{10}(OH)_8 + 7FeS_2 + 14As = 14FeAsS + 3SiO_2 + 4H_2O_{(l)} + 4O_{2(g)}$	250	-149.29	-148.76	-148.24
		300	-130.80	-130.48	-130.04
		350	-115.20	-115.01	-114.66
6.	$2Mg_5Al_2Si_3O_{10}(OH)_8 + \frac{14}{3}SiO_2 + \frac{8}{3}H_2O_{(l)} = \square_2Al_4Si_4O_{10}(OH)_8 + \frac{10}{6}Mg_6Si_4O_{10}(OH)_8$	250	-5.525	-5.368	-5.242
		300	-6.131	-5.953	-5.813
		350	-6.673	-6.475	-6.309
7.	$6Fe_2O_3 = 4Fe_3O_4 + O_{2(g)}$	250	-35.302	-35.270	-35.233
		300	-31.102	-30.985	-30.952
		350	-27.398	-27.378	-27.347

Calculated from free energy, heat capacity and molar volumes for chlorite components from Walshe (pers. comm.), for As from Robie *et al.* (1978), for arsenopyrite from Barton & Skinner (1979), a molar volume for arsenopyrite of 25.97 cm^3 $mole^{-1}$ (from cell measurements reported by Clark, 1960), and for other minerals, O_2 and S_2 from Helgeson *et al.* (1978). The values of the apparent free energy of formation for H_2O and the pressures on the liquid-vapour curve from Helgeson & Kirkham (1974) were used.

(b) ARSENOPYRITE-TENNANTITE

		log K (T in °K)
8.	$4FeAsS + 10CuFeS_2 + ZnS + 7S_{2(g)} = Cu_{10}FeZnAs_4S_{13} + 13FeS_2$	74090/T - 63.874 (T < 363°C) 73609/T - 63.132 (363 < T < 491°C)

Calculated from thermodynamic data in Barton & Skinner (1979) using the method of Craig & Barton (1973) - see text.

(c) DATA USED IN COMPUTATION OF $\Sigma SO_4/\Sigma H_2S$ versus T and pH (Fig. 8.1; Appendix 5).

		log K_T (T in °K) log K = A + B(10^4/T) + C(10^4/T)²			
		A	B	C	Source
9.	$H_2S = H^+ + HS^-$	-21.8359	1.1448	-0.02120	a
10.	$HS^- = H^+ + S^{2-}$	-21.4022	0.8979	-0.01950	a
11.	$2H^+ + SO_4^{2-} = H_2S_{(aq)} + 2O_{2(g)}$	51.09715	-6.2208	0.02950	a
12.	$HSO_4^- = H^+ + SO_4^-$	-19.0477	1.0026	-0.01495	a
13.	$KSO_4^- = K^+ + SO_4^{2-}$	-14.7077	0.9469	-0.01640	a
14.	$NaSO_4^- = Na^+ + SO_4^{2-}$	-14.7077	0.9469	-0.01640	a
15.	$CaSO_4^o = Ca^{2+} + SO_4^{2-}$	-16.2093	0.9106	-0.01505	a
16.	$MgSO_4^o = Mg^{2+} + SO_4^{2-}$	-14.3396	0.6749	-0.00940	a
17.	$H_2S_{(aq)} + \frac{1}{2}O_{2(g)} = H_2O_{(l)} + \frac{1}{2}S_{2(g)}$	-3.9973	1.0278	-0.00060	a
18.	$FeS_2 = FeS + \frac{1}{2}S_{2(g)}$	6.3611	-0.68857		b
19.	$3FeS_2 + 2O_{2(g)} = Fe_3O_4 + 3S_{2(g)}$	14.8401	1.0443	0.00177	a
20.	$2FeS_2 + \frac{7}{2}O_{2(g)} = Fe_2O_3 + 2S_{2(g)}$	5.5043	1.3466	-0.00377	a

		A	B	C	Source
21.	$3FeS + 2O_{2(g)} = Fe_3O_4 + 3/2 S_{2(g)}$	-7.6752	3.3989	-0.00193	a
22.	$6Fe_2O_3 = 4Fe_3O_4 + O_{2(g)}$	14.8949	-2.6110	0.00175	a
23.	$4FeS_2 + Cu_2FeS_4 = 5CuFeS_2 + S_{2(g)}$	12.560	-1.1067		a
24.	$BaSO_4 = Ba^{2+} + SO_4^{2-}$	8.8048	-0.33619	-2.5138 x 10^6xT^3	c
25.	$Fe_{4.5}Al_3Si_{2.5}O_{10}(OH)_8 + 1.5SiO_2 + K^+ + 9H_2S_{(aq)} + 3/4 O_{2(g)} = 3/2 FeS_2 + KAl_3Si_3O_{10}(OH)_2 + 23/4 H_2O_{(l)} + H^+$	-132.97	15.312	-0.15215	d
26.	$KAl_3Si_3O_{10}(OH)_2 + 10H^+ = K^+ + 3Al^{3+} + 3H_4SiO_4$	-18.041	0.6181	0.013112	d
27.	$KAlSi_3O_8 + 4H^+ + 4H_2O_{(l)} = K^+ + Al^{3+} + 3H_4SiO_4$	-4.9080	0.10427	0.0024635	d
28.	$Al_2Si_2O_5(OH)_4 + 6H^+ = 2Al^{3+} + H_2O_{(l)} + 2H_4SiO_4$	-10.585	0.1999	0.010861	d
29.	$SiO_2 + 2H_2O_{(l)} = H_4SiO_4$	-0.56398	-0.04973	-0.001652	d
30.	$KFe_3AlSi_3O_{10}(OH)_2 + 1/2 H_2O_{(l)} = KAlSi_3O_8 + 1.5Fe_2O_3 + 3H^+$	-6.2668	1.6024	0.0005916	d
31.	$NaAlSi_3O_8 + 4H^+ + 4H_2O_{(l)} = Na^+ + Al^{3+} + 3H_4SiO_4$	-5.7945	0.19136	0.002950	e
32.	$FeS_2 + 2H^+ + H_2O = Fe^{2+} + 2H_2S + 1/2 O_{2(g)}$	84.105	-9.0405	1.8484	h
33.	$FeCl^+ = Fe^{2+} + Cl^-$	29.037	-3.4355	0.093963	h
34.	$FeCl_2^0 = Fe^{2+} + 2Cl^-$	-5.7057	-1.1050	0.073536	h
35.	$CuCl^0 = Cu^+ + Cl^-$	-12.266	1.0001	-0.024881	i
36.	$Cu^+ + H_2S + HS^- = Cu(HS)_2^- + H^+$	-9.4727	0.19401	0.015912	i
37.	$Cu^+ + 2H_2S + HS^- = Cu(H_2S)(HS)_2^- + H^+$	10.118	-1.9635	0.0714	i
38.	$ZnS = Zn^{2+} + S^{2-}$	-35.456	1.2525	-0.02765	e
39.	$Zn^{2+} + Cl^- = ZnCl^-$	21.009	-1.1145	0.015912	e
40.	$Zn^{2+} + 2Cl^- = ZnCl_2^0$	24.482	-1.3516	0.019165	e
41.	$Zn^{2+} + 3Cl^- = ZnCl_3^-$	28.214	-1.5905	0.022913	e
42.	$Zn^{2+} + 4Cl^- = ZnCl_4^{2-}$	31.596	-1.8039	0.02603	e

Additional equilibria

43.	$H_2O = H^+ + OH^-$	$\log K_{43} = -6 \times 10^{-5}T^2(°C) + 0.0290\ T(°C) - 14.7226$	a
44.	$K_2Al_6Si_6O_{20}(OH)_4 + BaSO_4 + 2H^+ = Ba\ Al_6Si_6O_{20}(OH)_4 + H_2S_{(aq)} + 2O_{2(g)} + 2K^+$	$\log K_{44} = -144.36 + 2.1138 \times 10^5/T - 7.6201 \times 10^7/T^2 + 1.2497 \times 10^{10}/T^3$	f
45.	$2FeAsS + S_{2(g)} = 2FeS_2 + 2As$	$\log K_{45} = 13462/T - 13.4842$ T range 25-363°C	g
46.	$FeAsS + S_2 = FeS_2 + (As,S)_{(l)}$	$\log K = 11648/T - 10.6432$ T range 363-491°C	g
47.	$Ba^{2+} + Cl^- = BaCl^+$	$\log K_{47} = -10.6 + 1446/T + 0.019T$	j
48.	$CuFeS_2 + H^+ + 1/2 O_{2(g)} = FeS_2 + Cu^+ + 1/2 H_2O_{(l)}$	$\log K_{48} = -61.681 + 19193/T + 0.05819T$	i

Sources:

a Ripley & Ohmoto (1977, 1980).

b Calculated from the data of Scott & Barnes (1971), assuming an activity of FeS in pyrrhotite of 0.48 at the pyrite-pyrrhotite boundary at temperatures below 350°C (Craig & Scott, 1974), the relationship between mole % FeS and activity of FeS in sphalerite of Craig & Scott (1974), the activity of S_2 at the bornite-pyrite-chalcopyrite buffer of Schneeberg (1973) and the data of Czamanske (1974) on the iron content of sphalerite at the bornite-chalcopyrite-pyrite aS_2 buffer corrected to 1 bar pressure.

c Blount (1977).

d Program listing PD/REDOX/PH University of Tasmania by J.L. Walshe from data in Walshe (1977).

e Helgeson (1969).

f From equations 11,24, 26 and calculating a free energy of formation of □$BaAl_6Si_6O_{20}(OH)_4$ by the method of Tardy & Garrels (1974) using a value for the free energy of silication of BaO from the free energy data for $Ba_2Si_4O_7$ listed in Naumov *et al.* (1974).

g Barton & Skinner (1979).

h Crerar and Barnes (1976).

i Walshe and Solomon (1981).

j Drummond (1981).

Appendix 5

log ($\Sigma SO_4/\Sigma H_2S$) vs T and pH diagrams

These diagrams were constructed using a programme modified by J.L. Walshe, D.J. Patterson, M. Ahmad, A. Bush and the writer from a programme developed by Ripley & Ohmoto (1977, 1980). Thermodynamic data listed in Appendix 4 were used in the construction of the diagrams as well as the activity coefficient expressions of Patterson *et al.* (1981). The diagrams were useful in limiting the conditions of formation of the sulphide orebody. Boundaries between chlorite and annite and between these minerals and other silicates are based on end-member components $Fe_{4.5}Al_3Si_{2.5}O_{10}(OH)_8$ and $KFe_3AlSi_3O_{10}(OH)_2$ are gross approximations. The boundary between K-Ba mica and barite is based on reaction 33, Appendix 4.

$$K_{33} = \frac{a_{BaAl_6Si_6O_{20}(OH)_4} \cdot a_{H_2S} \cdot a^2_{O_2} \cdot a^2_{K^+}}{a_{K_2Al_6Si_6O_{20}(OH)_4} \cdot a^2_{H^+}}$$

which gives an expression for the stability field of barite without requiring an arbitrary assumption about the total molality of Ba in solution. A value of M_{K^+} must be assumed, but potassium concentration is commonly well constrained by the silicate mineralogy. The boundary was drawn assuming the following activity/composition relations

$$a_{Ba\text{-}mica} = X_{Ba\text{-}mica}$$
$$a_{K\text{-}mica} = X^2_{K\text{-}mica}$$

and a value of $X_{Ba\text{-}mica}/X^2_{K\text{-}mica}$ of 0.44 which corresponds to the high Ba-muscovite of sample 105174. In assemblages lacking barite, the Ba content of muscovite should give information on the maximum possible value of oxygen activity at any temperature.

Development of a solid solution model for muscovite similar to Walshe's chlorite model is clearly required for confident application of the approach, but must await experimental free energy determinations for Ba phyllosilicates.

The diagrams (Figs. A5.1-A5.5) are all constructed with the following solution compositions:

$$m_{K^+} = 0.1$$

$$m_{Na^+} = 0.9$$

$$m_{Ca^{2+}} = m_{Mg^{2+}} = 0.001$$

$$m_{Cl^-} = 1.0$$

Mineral abbreviations:

PO	pyrrhotite	K-Ba mica	barian muscovite
APY	arsenopyrite	ba	barite
PY	pyrite	ka	kaolinite
AS	arsenic	mu	muscovite
MT	magnetite	ab	albite
HT	hematite	chl	chlorite
K-mica	muscovite	ann	annite

Dotted lines: contours of mole % FeS in sphalerite.

Dot-dash lines: contours of $\delta^{34}S_{H_2S}$ assuming $\delta^{34}S_{\Sigma S} = 30\%$.

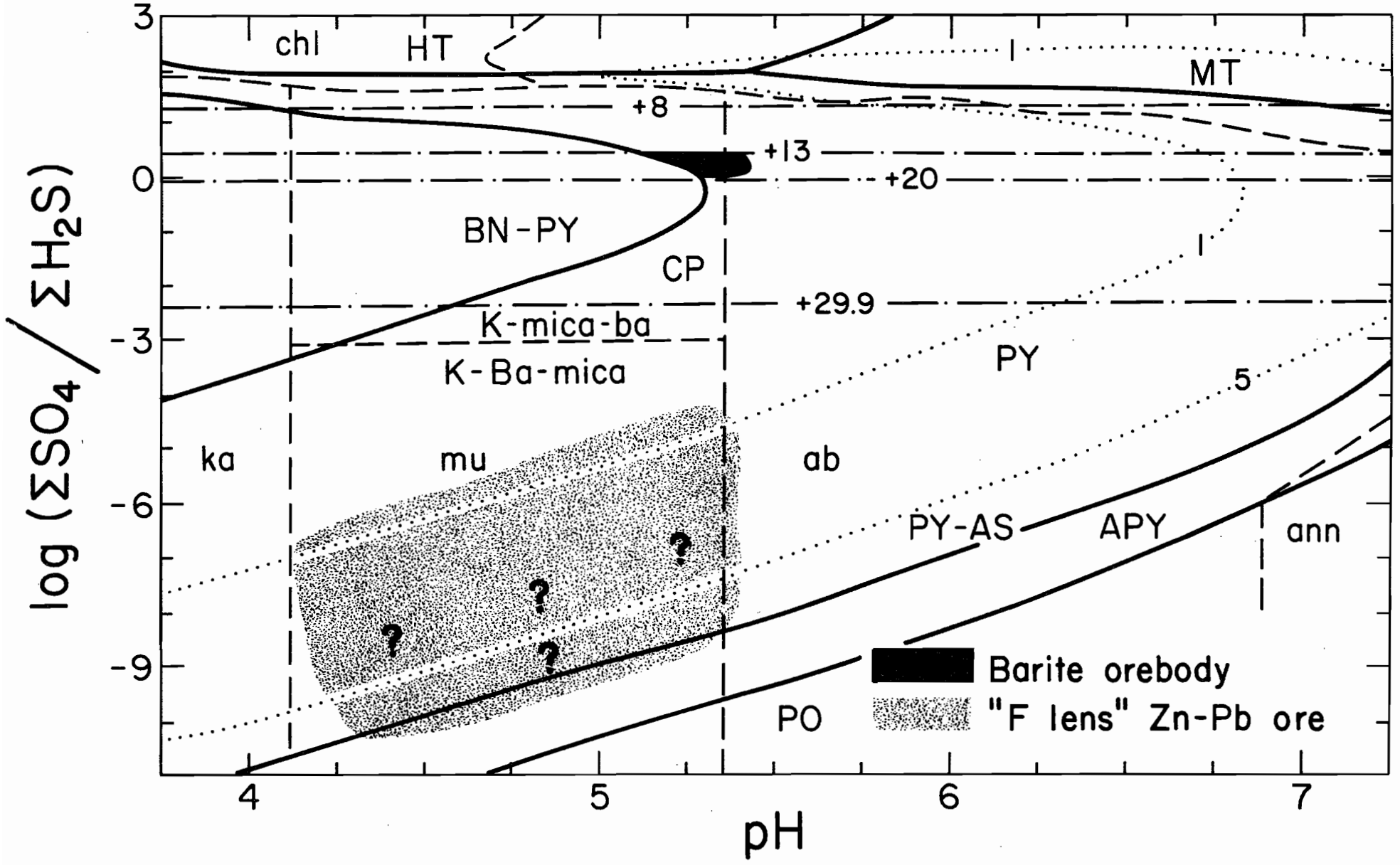

Fig. A5.1 log ($\Sigma SO_4/\Sigma H_2S$) versus pH diagram. T = 250°C. $m_{\Sigma S} = 10^{-2}$.

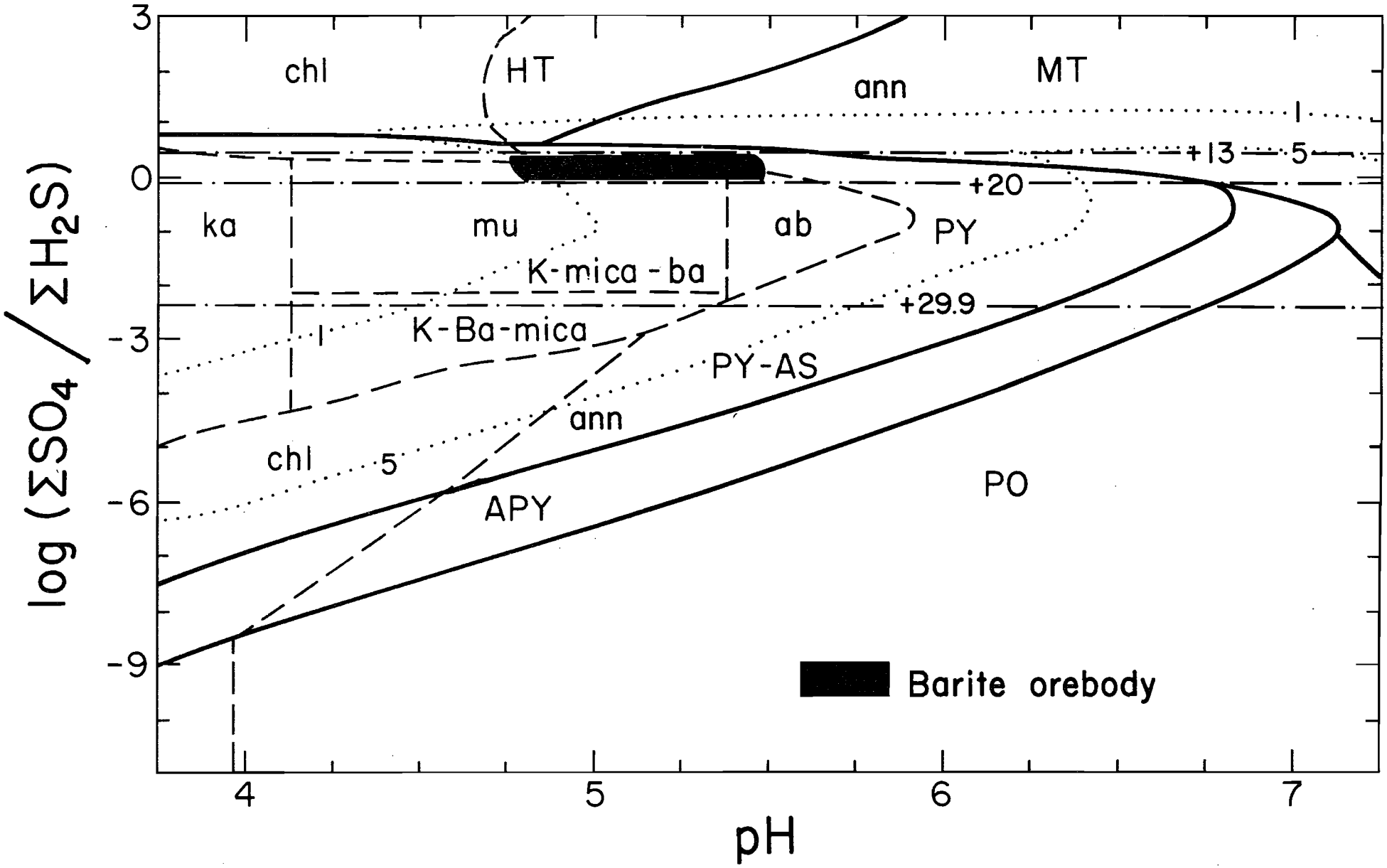

Fig. A5.2 log ($\Sigma SO_4/\Sigma H_2S$) versus pH diagram. T = 250°C. $m_{\Sigma S} = 10^{-3}$.

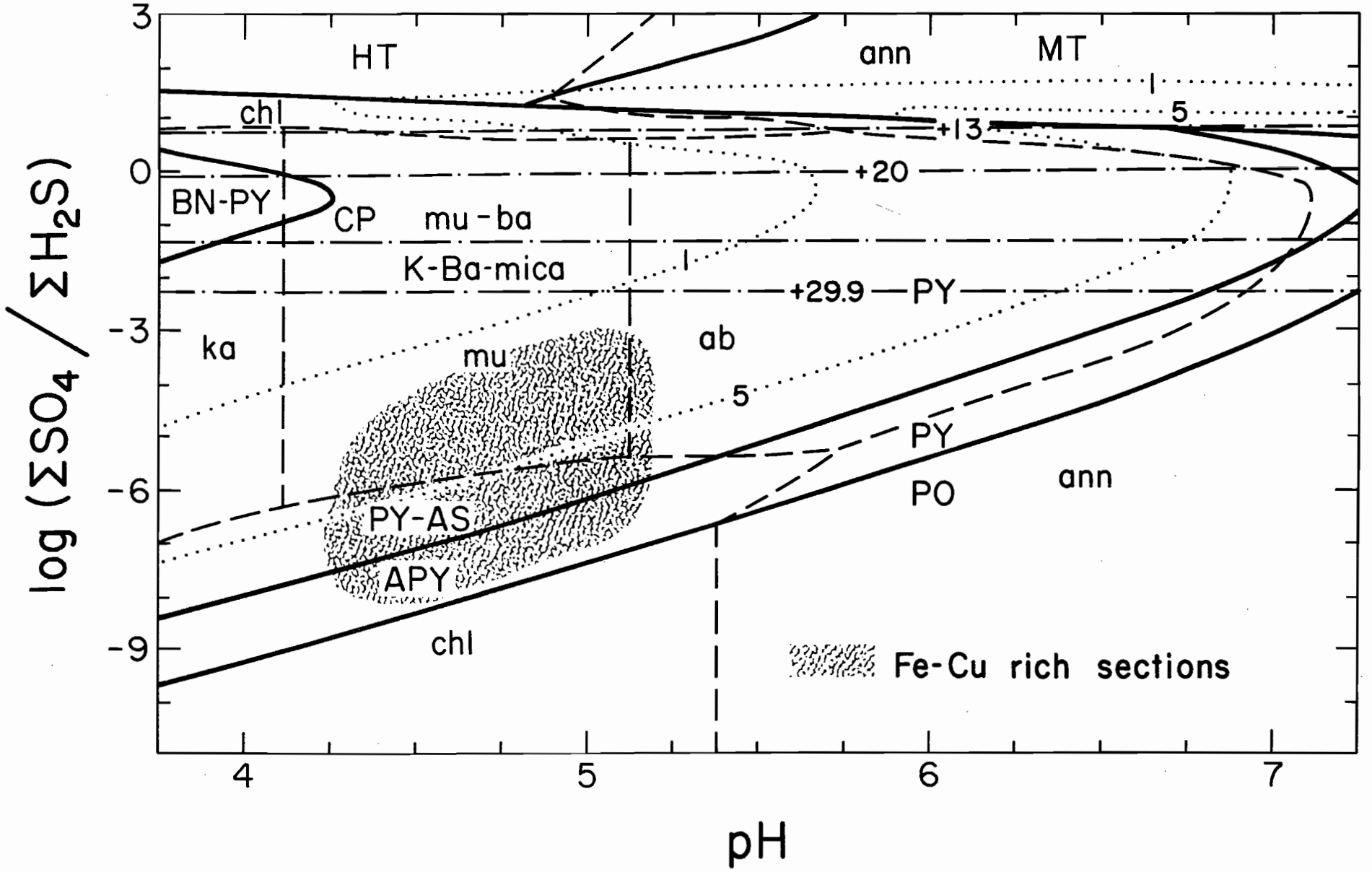

Fig. A5.3 log ($\Sigma SO_4/\Sigma H_2S$) versus pH diagram. T = 300°C. $m_{\Sigma S} = 10^{-2}$.

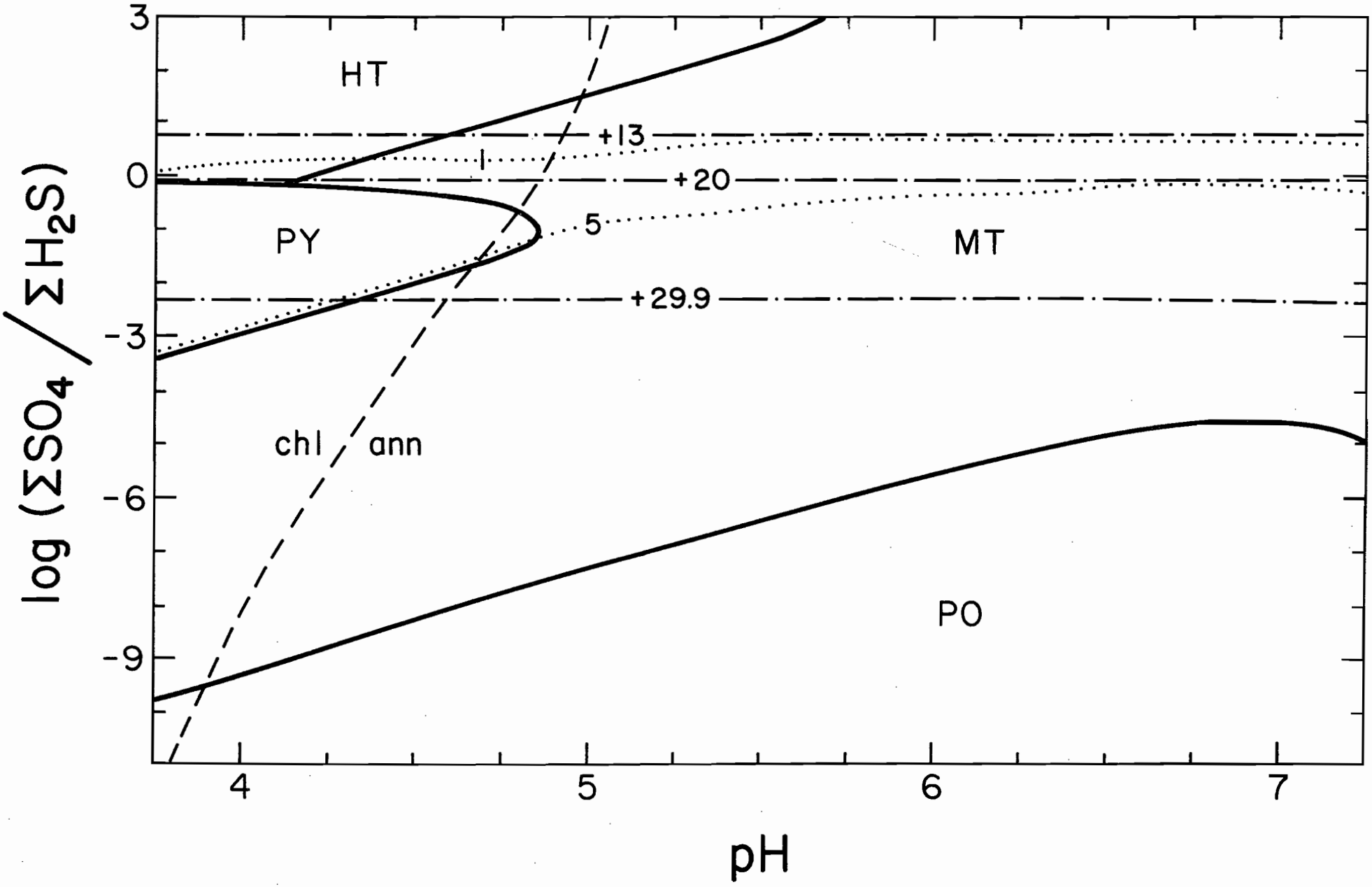

Figure A5.4 log ($\Sigma SO_4/\Sigma H_2S$) versus pH diagram. T = 300°C. $m_{\Sigma S} = 10^{-3}$.

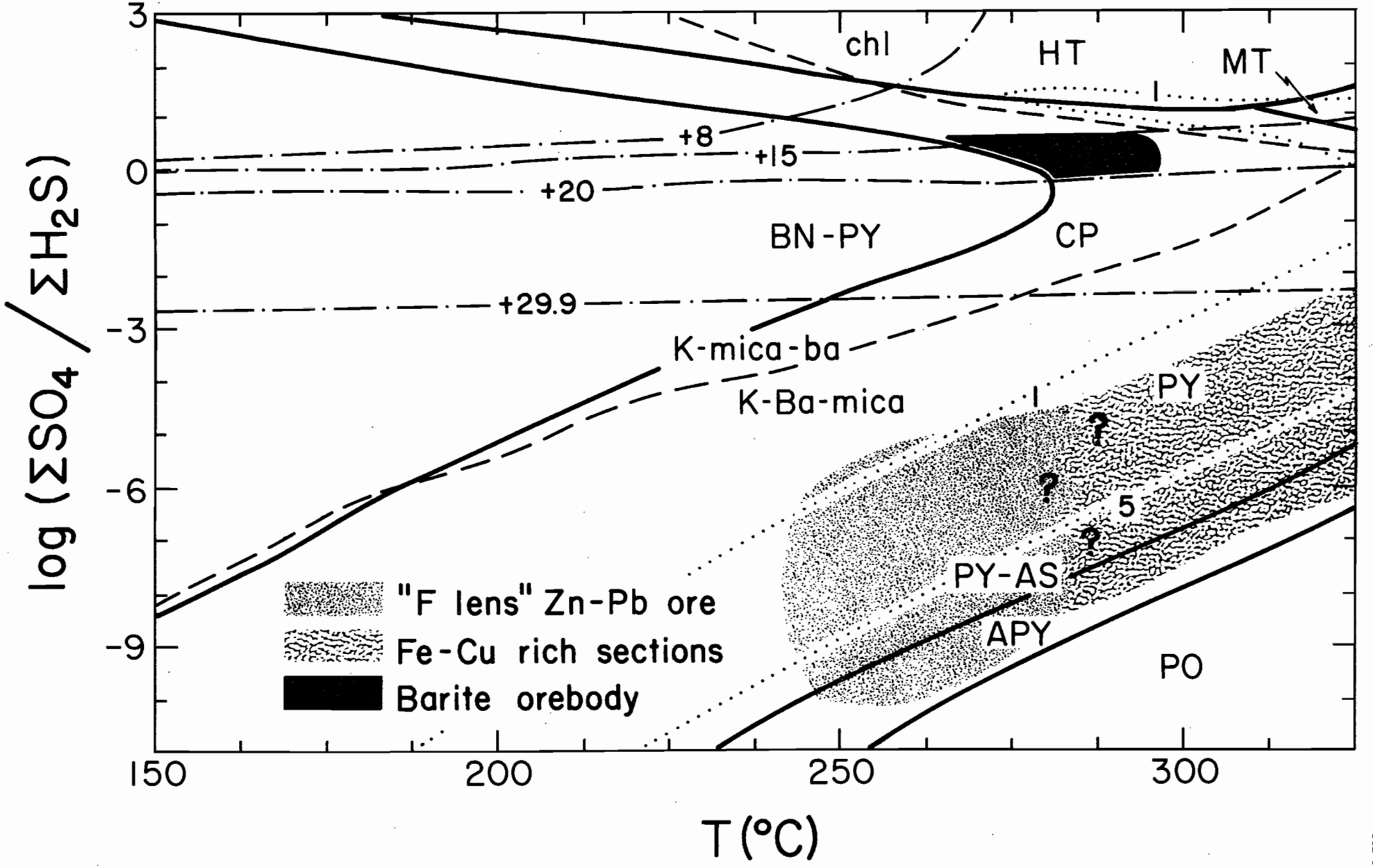

Fig. A5.5 log ($\Sigma SO_4/\Sigma H_2S$) versus T diagram. $m_{\Sigma S} = 10^{-2}$, pH 0.5 units acid.

Appendix 6

SULPHUR ISOTOPE GEOTHERMOMETRY

In this thesis the sulphur isotope geothermometers chosen by Ohmoto and Rye (1979) have been used, with the exception of the barite-H_2S fractionation which was chosen to be consistent with the 300°C fractionation factor, $\alpha^{SO_4^{2-}}_{H_2S}$ of 1.020 $\pm$ 0.0002 reported by Sakai and Dickson (1978). More recently Ohmoto and Lasaga (1982) and Robinson (1978)* have suggested alternative formulations of the fractionation equation:

$$1000\ ln\ \alpha^{SO_4}_{H_2S} = 6.04 \times 10^6/T^2 + 2.6 \quad \text{(Robinson)}$$

$$1000\ ln\ \alpha^{SO_4}_{H_2S} = 6.463 \times 10^6/T^2 + 0.56 \quad \text{(Ohmoto and Lasaga)}$$

Isotopic temperatures for Rosebery samples according to the three thermometers (Samples listed in Table 6.1) are tabulated below. The assumption is made that there is no fractionation between barite and SO_4^{2-}.

Table A6.1 Comparison of geothermometers of Rosebery barite rocks

	Isotopic Temperature (°C)		
Sample	This Thesis	Robinson	Ohmoto and Lasaga
33446	170	191	190
14446	255	271	264
33947 (gn)	278	293	284
33947 (sl)	297	313	300
33988	298	315	302
34989	277	295	285
34990	281	298	288

For samples from the barite orebody the temperatures calculated in this study agree within 9° with those calculated by the equation of Ohmoto and Lasaga. For sample 33446, from the sulphide orebody the geothermometers of Robinson (1978)* and Ohmoto and Lasaga (1982) are in good agreement, but the temperature calculated using the equation

on p. 6.12 (this thesis) is lower by 20°. This in no way affects the conclusion that sulphur isotope equilibration is unlikely at the indicated temperature and this is borne out by the textural evidence that the pyrite and barite of this sample were not co-precipitated in equilibrium.

Of the geothermometers it is believed that the one of Ohmoto and Lasaga (1982) is the best currently available. Ohmoto and Lasaga critically evaluated all available literature and with this data base, together with the unpublished results of experiments by Ohmoto and previously unpublished details of the experimental methods of Igumnov (1976)*, they established a kinetic model for the isotopic equilibration of SO_4^{2-} species and H_2S via a $S_2O_3^{2-}$ intermediate. Their model was able to satisfactorily explain a discrepancy between activation energies for the isotopic exchange reaction measured in very acidic (Robinson, 1973)* or in near neutral to alkaline solutions (Igumnov, 1976)* and was based on relating the exchange equilibria to the speciation of the solution at experimental conditions. This model is predictive, unlike the empirical formulations of Robinson (1973)*, Igumnov (1976)* and Sakai and Dickson (1978), but is subject to uncertainties in estimated high temperature ion pair stability constants.

Because of the good agreement between the barite-sulphide isotopic temperatures calculated using the empirical equation used in this thesis and published in Green *et al.* (1981) and those using the SO_4^{2-} - H_2S isotopic fractionation factors of Ohmoto and Lasaga (1982) and because the slight differences that do exist in no way affect the conclusion reached in the thesis it was decided to retain the published temperatures.

Ohmoto and Rye (1979) selected their values for the temperature dependence of isotopic fractionation among pyrrhotite, pyrite, sphalerite, galena, chalcopyrite, H_2S and HS^- purely from experimental data. For pyrite, chalcopyrite and pyrrhotite fractionation they selected the data of Kajiwara and Krouse (1971). For sphalerite and galena fraction-

ation they considered the experimental data of Kajiwara and Krouse (1971), Kiyosu (1973)*, Kajiwara *et al.* (1969)*, Salomons (1971)* and Czamanske and Rye (1974)* and chose what they considered to be the "best" value. It is unlikely that the experiments of Salomons (1971)* attained equilibrium. The results of various experiments and their methodology are tabulated in Table A6.2.

Table A6.2 Calibrations of sphalerite-galena isotopic fractionation

Study	Technique	Tra[2]	App.[3]	A[4]	B	200[5]	300
K *et al.*	Synthesis with S, annealing	150-600	-	1.0836	-0.52	4.32	2.78
G & S	"	350-690	-	0.652	-0.07	2.84	1.91
K & K	Heating sulphide pairs in sulphur or other a_{S_2} buffer	250-600	+	0.8	0	3.57	2.43
K	Sl-HS^- hydrothermal	50-150	+	0.891	-0.57	3.41	2.14
	gn-HS^- "	100-300					
C & R	Hydrothermal recrystallization in NH_4Cl solution of sulphide pairs in 10-15°C T gradient	275-600	+	0.7	0	3.13	2.13
Sch. *et al.*	Exchange of individual sulphides with NaHS solutions	217	-	0.77	0	3.44	2.34
Sm. *et al.*	Synthesis of py + sl+ gn with S, plus subsequent annealing	150-600	-	0.828	0	3.70	2.52
S	Theoretical calculation			0.963	0	4.30	2.93
H	"			0.765	0	3.42	2.33
E & H	"			0.856	0	3.82	2.61
G & P	"			0.9	-0.2	3.82	2.54
O & R	Compilation	50-700		0.73	0	3.26	2.22

1. K *et al.* = Kajiwara *et al.* (1969)*, G & S = Grootenboer and Schwarcz (1969)*, K & K = Kajiwara and Krouse (1971), K = Kiyosu (1973)*, C & R = Czamanske and Rye (1974)*, Sch. *et al.* = Schiller *et al.* (1970)*, Sm. *et al.* = Smith *et al.* (1977), S = Sakai (1968)*, H = J.R. Hulston in Groves *et al.* (1970)*, E & H = Elcombe and Hulston (1975)*, G & P = Golyshev and Padalko (1978)*, O & R = Ohmoto and Rye (1979).

2. Tra = temperature range in °C.

3. App = + if equilibrium was approached from starting materials with Δ values both greater than and less than the equilibrium value. Otherwise App = -

4. $1000\ ln \alpha^{sl}_{gn} = 10^6\ A/To_K^2 + B$

5. Calculated Δ values at 200 and 300°C.

Study of the various experiments indicates that the rates of sulphur isotope exchange are higher in the hydrothermal experiments than in experiments where sulphides are heated with elemental sulphur which in turn are higher than experiments where sulphides are heated together. Further, the rates of reaction vary with experimental technique. Thus, for example, in metal sulphide sulphur systems the rate of equilibration would appear to be gn>sl>py (Kajiwara and Krouse, 1971), whereas in metal sulphide HS^- systems sphalerite equilibrates quicker than galena (Kiyosu, 1973). Incidentially, there appears to be a curious systematic error in the reporting of Kiyosu's data. He assumed first order kinetics for sphalerite HS^- and galena HS^- exchange. Thus:

$$ln\ (1-f) = -Kt \qquad \text{(Kiyosu, 1973, eq.9)}$$

where f is fraction of sulphur isotopic exchange

K is exchange rate constant

t is time

At f = 0.5 (50% exchange):

$t_{\frac{1}{2}} = 0.693/K$, where $t_{\frac{1}{2}}$ is half time of exchange

It is found by examination of Kiyosu's Table 4, that the half times of exchange values are too high by a factor of about 5.2 compared with those calculated from the value of K. Since the tabulated values of K are consistent with those of f, it will be assumed that the values of log $t_{\frac{1}{2}}$ (Kiyosu, Table 4) are low by 0.72 (log hours). Even so, these results appear to provide some of the best data, in that high degrees of isotopic exchange were achieved ($\geqq 0.48$), equilibration appeared to be approached at low temperatures and only two phases were reacted together at a time. In other experiments, three or more phases were reacted together. This presents the difficulty that if phase A reacts more quickly than phase B a change in the $\delta^{34}S$ of phase A during the experimental run might occur with the isotopic composition of B remaining constant for a time and then starting to change. Such an experiment, if terminated too quickly, might give a false impression

of approach to equilibrium. Such an effect might have occurred in some of the runs of Kajiwara and Krouse (e.g. Fig. 6, 600°C; Fig 12, 500°C). Of course, the more phases present, the greater the chance of this effect occurring. This makes the experiments of Smith *et al* (1977)*, where 5 phases (py, sl, gn, liquid and vapour phase S) might have been present, particularly difficult to interpret. This effect could even affect the hydrothermal experiments of Czamanske and Rye (1974)* which involved recriptallization of sphalerite and galena in NH_4Cl solutions in a temperature gradient. Likely problems in this study include:

i. The presence of a temperature gradient in these experiments indicates that irreversible behaviour may have occurred.

ii. If say, sphalerite was mobilised before galena and continued to exchange after participation faster than galena (c.f. Kiyosu, 1973), these effects together with Rayleigh fractionation effects (because of the limited initial sulphur supply) could yield spurious results.

iii. The exchange medium might play an important part. For example, Czamanske and Rye noted an inverse order of isotopic fractionation ($\Delta^{sl}_{gn} < 0$) and a change in crystal morphology (octahedral vs. cubic habit of galena) when NH_4I solutions were used instead of NH_4Cl. Such effects are reminiscent of the importance of adsorption effects in hydrothermal sulphur isotope fractionation suggested by Yaroshevich and Tvalchrelidze (1981)* and discussed in Chapter 6.

Despite these concerns it is apparant that the experiments of Czamanske and Rye are some of the more reliable of those attempted, in that equilibrium was approached from both Δ^{sl}_{gn} values being less than, and, greater than, the equilibrium value at the start. Other well documented experiments include those of Kiyosu (1973)*, Kajiwara and Krouse (1971) and Schiller *et al.* (1970)*. It is apparant that the experiments of Grootenhoer and Schwarcz (1969)* did not reach equilibrium. Perhaps the best experimental data might be reached in "dry"

systems at temperatures greater than 400°C (to avoid re-equilibration problems during quenching) and hydrothermal systems at lower temperatures (because of faster reaction rates).

Of the theoretical calculations, that of Hulston (in Groves *et al.*, 1970)* agrees best with the preferred experimental data. Further, it is likely that the true equilibrium fractionation lies somewhere between the experimental results of Czamanske and Rye (1974)* and Kajiwara and Krouse (1971). Most investigators appear to have constrained their experimental curves to pass through the origin of a plot of 1000 $ln \alpha$ vs. $^{1}/_{T\ (^{o}K)^{2}}$ consistent with the thermodynamics of isotope exchange (Bigeleisen and Mayer, 1947*; Urey, 1947*). Exceptions are the studies of Kajiwara *et al.* (1969)*, Grookenboer and Schwarcz (1969)* and Kiyosu (1973)*. Kiyosu's calibration agrees better with that of Czamanske and Rye (1974) at 300°C and with that of Kajiwara and Krouse (1971) at 200°. Hence, the compilation of Ohmoto and Rye (1979) is a good reflection of the current state of knowledge. Such a conclusion is not inconsistent with the results of studies which compared sulphur isotope geothermometry with either fluid inclusion filling temperatures in ore deposits (Groves *et al.*, 1970;* Rye, 1974)* or with temperatures in currently active geothermal systems (Browne *et al.*, 1975)*.

These studies suggest that an approach to sulphur isotopic equilibrium might be achieved during sub-surface sulphide deposition. The study of Kerridge *et al.* (1983)* indicates that kinetic effects probably predominate during ore deposition from exhalative hydrothermal solutions. Thus, it is probable that the partial sulphur isotope equilibration at Rosebery might reflect approach, but not attainment, of equilibrium during metamorphism from an initial disequilibrium situation via a solid-state diffusion process. On the other hand the coarse grained pyrite-pyrrhotite assemblages might have achieved equilibrium during post tectonic hydrothermal metasomatism and recrystallization (*c.f.* Kuroko; Eldridge, 1981*, Kajiwara, 1971).

GEOLOGY OF
THE ROSEBERY AREA

G. R. GREEN B.Sc (Hons.)

0 — 1 — 2 KILOMETRES

0 — 1 MILE

QUATERNARY

Undifferentiated glacial, fluvioglacial, periglacial and fluvial deposits. Man-made deposits indicated (black stippled overprint)

CAMBRIAN?

Acid intrusive rocks, mainly quartz-feldspar porphyry.

Mafic to intermediate, generally fine grained, intrusive rocks.

MOUNT BLACK VOLCANICS

Crystal tuff and lava of andesite to dacite composition Agglomerate indicated (A)

Massive, flow-banded, and autoclastic plagioclase-phyric rhyolite lava, with minor pyroclastic units. Breccias indicated (△).

PRIMROSE PYROCLASTICS

Massive pyroclastics

Vitric, crystal and lithic tuff and breccia of mainly rhyolite composition. Shale-sandstone horizons indicated (blue); breccias indicated (△). Quartz-phyric rocks indicated (Q).

North Pieman Area

Quartz-feldspar bearing, graded breccia to banded tuff, units

Dacite crystal tuff.

Host Rock and correlates

Black slate-siltstone-sandstone horizons. Volcanic horizons indicated ( ). Quartz-phyric volcanic rocks indicated (Q)

Footwall pyroclastics

Dominantly ignimbritic rhyolite feldspar-phyric vitric-crystal-lapilli tuff. Zones of quartz-sericite + chlorite + carbonate + pyrite schist indicated (diagonal overprint).

MOUNT READ VOLCANICS

CRIMSON CREEK FORMATION CORRELATE

Maroon or green shale-mudstone sequence with horizons of mafic volcaniclastic sandstone.

ROSEBERY GROUP

Black slate, quartz wacke sandstone. Minor dolomite units indicated (d) (Munro Creek Slate).

Quartz-phyric rhyolite tuff (Williamsford Volcanics).

Quartz-phyric rhyolite tuff and breccia (Natone Volcanics).

Polymict, fuchsite-bearing, conglomerate and sandstone (Salisbury Conglomerate).

Dolomitic siltstone and shale, minor slide conglomerate units indicated (stipple), minor sandstone (Westcott Argillite)

Quartz wacke, lithic wacke, black slate. Minor conglomerate (Stitt Quartzite). Strongly deformed zone indicated (diagonal stripes)

Black slate with acid volcaniclastic sandstone indicated (stipple) (Chamberlain Shale).

Geological boundary-observed. Dip shown by tick where measured.

Geological boundary - approximate.

Geological boundary - inferred

Fault, approximate

Fault, inferred

Strike and dip of bedding. Facing known from sedimentary features. 60

Strike and dip of overturned bedding. Facing known from sedimentary features. 40

Strike and dip of bedding. Facing unknown. 50

Strike and dip of primary foliation in volcanic rocks. 60

Strike and dip of slaty cleavage, spaced cleavage in volcanic rocks. 50

Vertical cleavage.

Strike and dip of crenulation cleavage. 50

Axial trace of major anticline, syncline, observed.

Axial trace of major anticline, syncline, approximate.

Axial trace of major anticline, syncline, inferred.

Axial trace of inferred faulted anticline.

Axial trace of overturned syncline.

Minor fold, early generation with plunge, dip of axial surface shown. 10/70

Minor fold, later generation with plunge, dip of axial st surface shown. 10/60

Minor fold with dextral, no, sinustral asymmetry looking down plunge.

Prospect or abandoned mine

Mine

Diamond drill hole

CONTOUR INTERVAL 100 METRES

BASE MAP ADAPTED FROM ELECTROLYTIC ZINC CO. COMPILATION.

Geology by G.R. Green except for Pieman River east of 80500 E (Anderson, 1972) and Rosebery Group — Mt Read Volcanics contact north of 79000 N (from Barton et al., 1966).

HINGE ZONE OF MAJOR SYNCLINE, PIEMAN RIVER